

SYN-LUNGS: Towards Simulating Lung Nodules with Anatomy-Informed Digital Twins for AI Training

Fakrul Islam Tushar, Lavsén Dahal, Cindy McCabe, Fong Chi Ho, Paul Segars, Ehsan Abadi, Kyle J. Lafata¹, Ehsan Samei, Joseph Y. Lo

Center for Virtual Imaging trials, Dept. of Radiology, Duke University Medical Center
Dept. of Electrical and Computer Engineering, Pratt School of Engineering, Duke University

Abstract. AI models for lung cancer screening struggle with data scarcity, limiting generalizability and clinical applicability. Generative models for image synthesis are constrained by training data variability. We introduce SYN-LUNGS, a framework for generating high-quality 3D CT images with detailed annotations. SYN-LUNGS integrates XCAT3 phantoms for digital twin generation, X-Lesions for nodule simulation (varying size, location, appearance), and DukeSim for CT image formation with vendor and parameter variability. The dataset includes 3,072 nodule images from 1,044 simulated CT scans, 512 lesions, and 174 digital twins. Effectiveness was shown for nodule detection, segmentation, cancer classification, and synthesis. Models trained on clinical + simulated data outperform clinical-only models, with 10% improvement in detection, 2–9% in segmentation, 2–9% in classification and enhanced synthesis. By integrating anatomy-informed simulations, this work facilitates future AI model development such as for rare disease representation and model reliability.

Keywords: Digital Human Twin · Segmentation · Computed Tomography · Simulated Nodule · Detection · classification · Synthesis.

1 Introduction

Computer-aided detection and diagnosis systems powered by deep learning are crucial for lung cancer screening, yet they remain limited by data scarcity, especially for rare cases [1,2,3]. Lung nodules vary widely in size, shape, and type, yet real-world datasets lack rare cases, segmentation masks, and diagnostic labels, limiting AI training [4,5,6,7,8]. Expert annotation is costly and time-consuming, while privacy concerns further restrict data sharing. To address these challenges, diffusion-based generative models have been explored for medical image synthesis [3,9]. While promising, they often lack anatomical and pathological constraints, failing to capture the full diversity of lung nodules or rare disease cases. Additionally, most image synthesis studies do not address the need to constrain for clinically relevant imaging scenarios.

To overcome the limitations of existing datasets and generative models, we introduce SYN-LUNGS, a physics- and anatomy-informed framework for generating simulated lung CT images to enhance AI model training. Unlike traditional generative models, SYN-LUNGS integrates digital human twins, procedural lesion modeling, and physics-based imaging simulation to improve anatomical and pathological fidelity. Using publicly available XCAT3 phantoms [10], we generate digital twins, embedding synthetic lung nodules with controlled size (4-30 mm), location, and appearance through X-Lesions [11,12]. DukeSim [13] ensures imaging realism by introducing scanner-specific variations, replicating vendor and acquisition differences. We evaluated SYN-LUNGS in nodule detection, segmentation, classification, and AI-based synthesis, demonstrating its impact on model generalization and robustness. In **related work**, phantom modeling has advanced from single-organ simulations such as for breast imaging to whole-body models, expanding their applications in CT for imaging protocol optimization, performance evaluation, disease quantification, and in-silico trials [15,16]. This evolution has enabled broader use in imaging research, including comparative analysis of imaging tools, AI-driven diagnostics evaluation [15,12,17,16]. To the best of our knowledge, this is among the first works integrating a digital human model with simulated lung nodules and physics-based CT simulation to enhance AI performance across multiple lung cancer diagnosis tasks. To summarize, this paper makes the following contributions:

1. We introduce SYN-LUNGS, a framework that synthesizes lung nodules by integrating anatomy-informed digital twins with imaging simulations. We generated anatomically and pathologically diverse digital human twins using the XCAT3 phantom family, incorporating controlled anatomical, pathological, and demographic variations. We employed the X-Lesions tool to procedurally generate synthetic lung nodules while ensuring realistic lesion characteristics before embedding them into digital twins. We applied DukeSim, a physics-based imaging simulator, to model realistic CT acquisition physics, ensuring synthetic nodules maintain consistency with real-world imaging.
2. We evaluate SYN-LUNGS across multiple downstream tasks, demonstrating that models trained on clinical + simulated data outperform clinical-only models, achieving better generalization and robustness in AI model training.

2 Method

Fig. 1 provides an overview of the SYN-LUNGS workflow, including dataset generation, downstream tasks, and evaluation metrics. The following sections provide detailed descriptions of digital human modeling, nodule simulation, imaging simulation, and the final dataset composition.

2.1 Digital Human Twins

We used the **XCAT3 phantoms** [10] to develop digital human twins, curating anatomical models from clinical chest CT scans. Instead of direct image

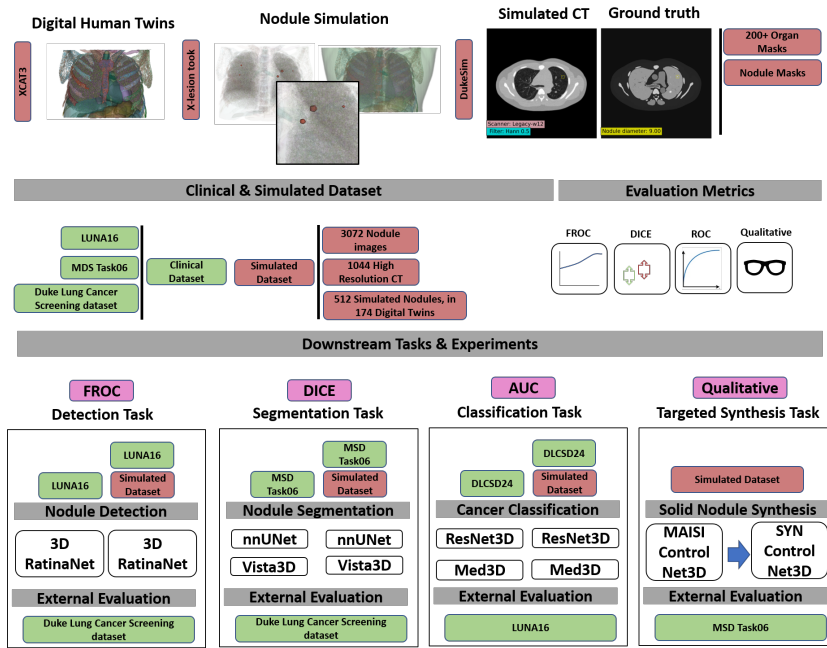


Fig. 1. Overview of the SYN-LUNGS workflow, integrating XCAT3, X-Lesion, and DukeSim for digital twin and nodule simulation. Clinical and simulated datasets are used for nodule detection, segmentation, classification, and synthesis, with external evaluations using FROC, DICE, AUC, and qualitative analysis.

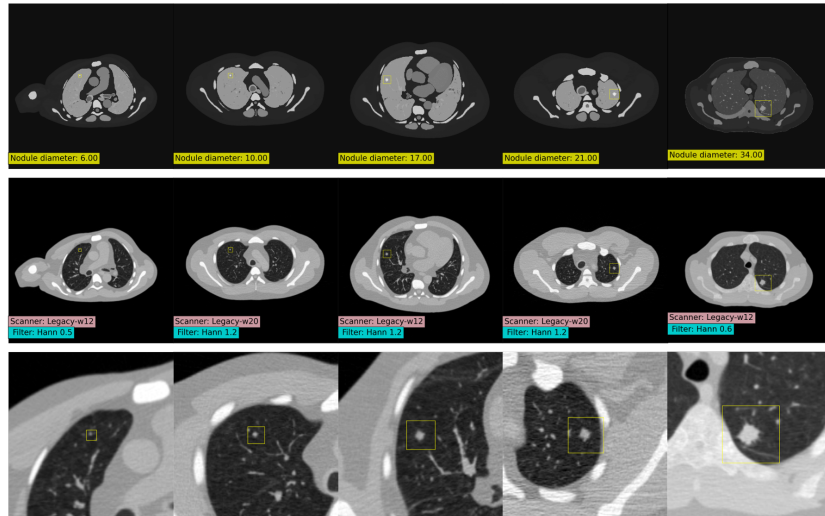


Fig. 2. Simulated lung nodules with varying sizes and imaging conditions. Top: digital human twins model slices with embedded nodules. Middle: simulated CT with different scanner settings. Bottom: zoomed-in nodule views.

synthesis, this structured pipeline integrates AI-driven segmentation and procedural texture modeling to generate anatomy-informed representations. The process began with nnU-Net segmentation using DukeSeg to delineate over 200 anatomical structures. A multi-step quality control process ensured anatomical fidelity, including statistical validation, anomaly detection, and physician review. Following segmentation, procedural modeling generated tissue textures such as lung vasculature, airways, and trabecular bone structures [18,19,20]. Each tissue type was mapped to its material properties to facilitate the next step for physics-based simulations. The axial slices of the digital human twins are shown in Fig. 2.

2.2 Nodule Simulation and Embedding

We utilized the **X-Lesions tool** [11,12] to generate and embed simulated lung nodules into digital human twins. Nodules were created at 0.1 mm voxel resolution, with controlled size, shape, and density. Internal heterogeneity of texture was introduced by the 3D clustered lumpy background (CLB) model [12]. Lesion sizes were drawn from a gamma distribution based on NLST [4] nodule data,

$$f(\ell_s|a, b) = \frac{b^a}{\Gamma(a)} \ell_s^{a-1} e^{-b\ell_s}, \quad \ell_s > 0 \quad (1)$$

where ℓ_s represents lesion size, and a, b are shape and scale parameters. This pipeline ensures a robust, enriched distribution. Fig. 2 shows axial slices of digital twins with embedded nodules.

2.3 CT Simulation

After embedding simulated nodules into digital human twins, CT imaging was performed using DukeSim [13], a validated simulation tool employing ray tracing for primary signals and Monte Carlo simulation for scatter and radiation dose. CT projections were reconstructed using a vendor-neutral MCR toolkit, replicating two representative scanners. The W12 scanner had 12 mm collimation, 570 mm source-to-isocenter distance (SIsoD), 1040 mm source-to-detector distance (SID), 16-channel detectors (1.5 mm width), and 7° anode angle. The W20 scanner featured 20 mm collimation, 541 mm SIsoD, 949 mm SID, 16-channel detectors (2.19 mm width), and 8° anode angle. Both scanners acquired 1,000 projections per scan using Hann 0.5, 0.6, and 1.2 reconstruction filters. Fig. 2 presents examples of simulated CT images.

2.4 Simulated dataset

The SYN-LUNGS dataset consists of 174 digital human twins with 512 simulated lung nodules, generating **1,044 CT scans and 3,072 nodule images** across the two scanners. Each scanner contributed 522 CT scans and 1,536 nodule images, ensuring coverage of diverse imaging conditions. The dataset includes 95

males (54.6%), ages 59 ± 15 years, with a mean BMI of 26 ± 6 . The cohort is 73.6% White, 20.7% Black, and 5.8% Other/Unknown, with 98.3% identifying as non-Hispanic. Unlike LUNA16 [5] and DLCSD24 [7,6], which provide 3D bounding boxes, only MSD Task06 [8] and SYN-LUNGS include 3D segmentation masks. While NLST [4] lacks segmentation, it provides malignancy labels. SYN-LUNGS incorporates statistically derived malignancy labels, adapted from prior studies [25]. Among the 174 digital twins, 124 were used for AI model training, while 50 were reserved as a test set. Performance was evaluated on internal and external datasets to assess how clinical + simulated training improves model generalization and robustness.

3 Downstream Tasks and Experiments

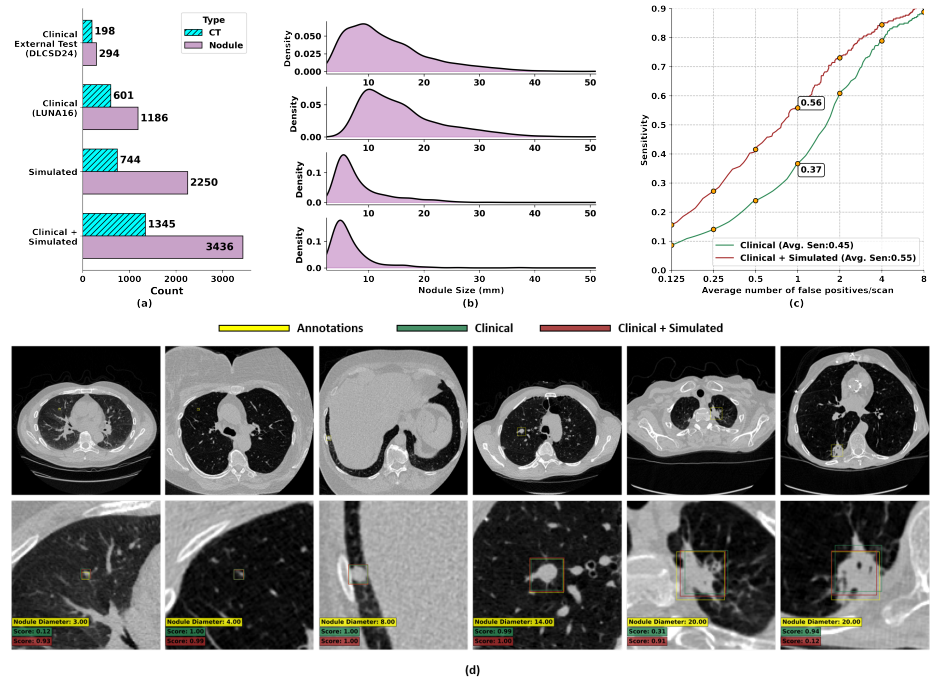


Fig. 3. Dataset Distribution and Detection Performance. (a) CT scan and nodule distribution. (b) Nodule size density plots. (c) FROC curve: clinical (green) vs. clinical + simulated data (brown). (d) Detection results with axial CT slices (top) and zoomed-in views (bottom), showing nodule size and confidence scores.

3.1 Nodule Detection

Nodule detection is a key step in lung cancer screening. To evaluate the impact of simulated data on AI model performance, we integrated clinical and simulated datasets into an open-source nodule detection pipeline. For training, we used LUNA16 [5], which includes 600 CT scans with over 1,000 annotated nodules, and 744 simulated CT images with varying imaging configurations to enhance dataset diversity. Fig. 3 shows the datasets and the nodule size distribution. Adding simulated dataset significantly enriches the number of images and nodule varying sizes. Two models were trained: one on clinical data only and another on a **clinical + simulated** dataset to assess the effect of synthetic augmentation. Performance was reported on the DLCSD24 open-access test set [7,6]. We employed the MONAI detection model [21], a widely used two-stage pipeline with region proposal networks (RPNs) and refined classification. The clinical + simulated model shows higher sensitivity across all false-positive rates, with an average sensitivity improvement from 0.45 to 0.55. Highlighted points indicate sensitivity at selected false-positive thresholds (Fig. 3(c)). Fig. 3(d) shows the nodule detection results of the model across different sizes.

3.2 Nodule Segmentation

Nodule segmentation is crucial in lung cancer screening, providing precise lesion boundaries for diagnosis. To evaluate the impact of simulated data, we integrated clinical and simulated datasets into an open-source segmentation pipeline, comparing models trained on clinical only and **clinical + simulated** data to assess segmentation accuracy and generalization. Fig. 4(a) shown the datasets and noduel size distribution associated to this experiment. We fine-tuned Vista3D [1] using MSD Task06 [8] as the primary clinical dataset and evaluated its generalizability on DLSC (validation dataset) [7], where voxel-wise annotations were unavailable. Performance was assessed within bounding box regions of detected nodules. Additionally, we trained nnUNet(v2) [24] on the same datasets, but unlike Vista3D, it lacked pretrained weights, requiring training from scratch.

The segmentation performance was evaluated on both the internal MSD Task06 test dataset [1](Fig. 4(b,c)) and the external DLCSD24 dataset(Fig. 4(d,e)). As shown in Fig. 4, models trained with **clinical + simulated** data demonstrated improved segmentation compared to those trained on clinical data alone. Vista3D and nnUNet models fine-tuned and trained with clinical + simulated datasets consistently outperformed their clinical-only counterparts across different nodule sizes. Performance gains were particularly notable for **smaller nodules (<10 mm)**, where the inclusion of simulated data enhanced Dice scores. Qualitative results in Fig. 4(f) further illustrate the segmentation improvements, with better alignment between predicted and ground truth boundaries.

3.3 Cancer Classification

Classifying lung nodules is challenging due to overlapping features. We trained models on clinical-only and **clinical + simulated** datasets, evaluating them on

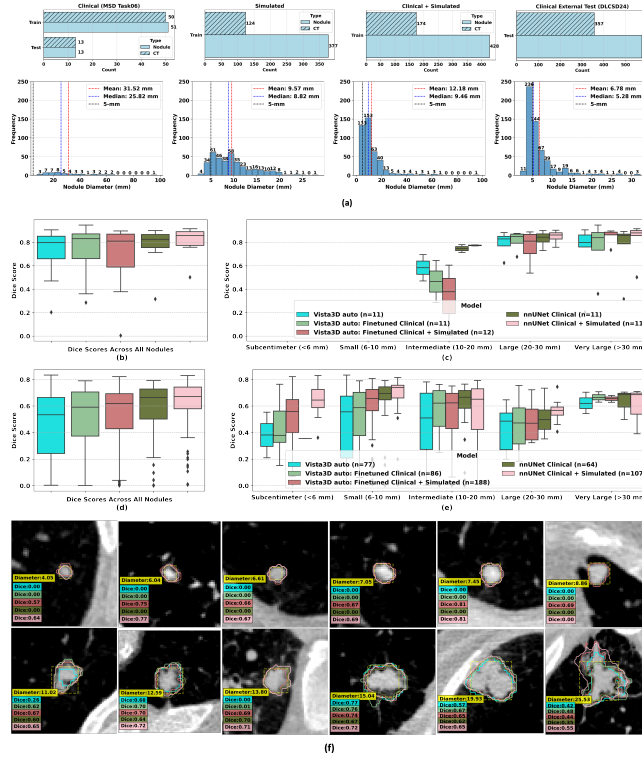


Fig. 4. Nodule Segmentation dataset(a) and performance(b-f). (a) Histograms of nodule size distributions across datasets, with mean (red), median (blue), and 5-mm threshold (black) dashed lines for reference. (a-d) Box plots compare Dice scores across models and datasets: (b, c) MSD Task06 (internal) and (d, e) DLCSD24 (external). Left: all nodules; right: clinically significant sizes. Legends show segmented nodule counts. (f) Qualitative examples with nodule diameter and Dice scores.

an external clinical dataset (Fig.5). The DLCSD24 dataset included 1,452 benign and 166 malignant nodules for training, and 510 benign and 65 malignant for validation [7,6]. From the simulated dataset, 366 nodules (1/4 of the clinical training set) were randomly selected from 290 synthetic CTs. Malignancy labels were assigned using a statistical model adapted from prior work [25], incorporating additional nodule features. Fig.5(a) illustrates the labeling process, where a logistic regression model trained on NLST [4] CT Set-1 predicted malignancy based on patient (age, sex) and nodule (size, margin, location, type) features. Fig.5(b) shows its AUC and 95% CI, ensuring reliability across datasets. For external evaluation, 677 LUNA16 nodules were used, adopting the Radiologist-Visual Assessed Malignancy Index (RVAMI) diagnoses [22,7] (Fig. 5(c)). We trained 3D ResNet50 [7] from scratch and fine-tuned pre-trained state-of-the-art MedicalNet’s ResNet50 (MedNet3D) [23]. All CT volumes were resampled

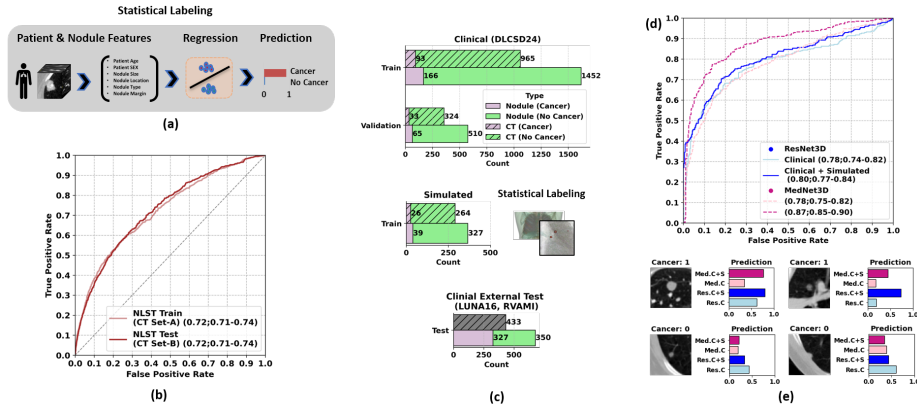


Fig. 5. Cancer Classification experiment workflow.(a)Statistical labeling, (b)Statistical labeling evaluation,(c)Dataset distribution,(d)Classification performance AUC and (e)score.

to $0.7 \times 0.7 \times 1.25$ mm, with intensity values clipped (-1000 to 500 HU) and standardized. Nodules were extracted as $64 \times 64 \times 64$ patches, and all models were trained for 200 epochs, selecting the best-performing model based on validation AUC. Fig.5(d) compares AUC-ROC curves, showing improved performance with simulated data. The ResNet3D clinical model achieved 0.78 (95% CI: 0.74–0.82), improving to 0.80 (0.77–0.84) with simulated dataset. MedNet3D saw greater gains, increasing from 0.78 (0.75–0.82) to 0.87 (0.85–0.90). Fig.5(e) highlights classification score distributions, showing better prediction agreement with clinical + simulated training.

3.4 Targeted Synthesis

Generative models have shown promising results in medical imaging, but their effectiveness is often limited by training data and the ability to control imaging features. The **MAISI foundational generative model** introduced ControlNet [3], allowing control over body region and size without requiring explicit masks. However, for targeted abnormality generation, such models are restricted by the availability of diverse pathological data. SYN-LUNGS addresses this gap by providing simulated images, facilitating controlled lesion synthesis. In this study, we developed **SYN-ControlNet**, an adaptation of MAISI’s ControlNet [3], fine-tuned exclusively on simulated solid nodules from SYN-LUNGS. By leveraging MAISI’s pretrained VAE and diffusion models, SYN-ControlNet enhances targeted type of nodule synthesis. This fine-tuned model enables control over nodule size, and anatomical placement, supporting both clinical and augmented nodule masks (Fig. 6). Fig. 6 illustrates the targeted synthesis approach leveraging MAISI and our fine-tuned SYN-ControlNet. Fig. 6(a) represents the finetuning of the original MAISI framework. Fig. 6(b) demonstrates the infer-

ence pipeline utilizing developed SYN-ControlNet, where clinical or augmented nodule masks are used to generate synthetic CT scans, enhancing control over nodule type and placement. Fig. 6 (c) provides a comparative visualization, synthetic CTs generated by MAISI-ControlNet (2nd column) and SYN-ControlNet (3rd column) respectively. These results highlight the role of simulated data in advancing generative models for medical imaging, enhancing their control, and applicability in clinical AI research.

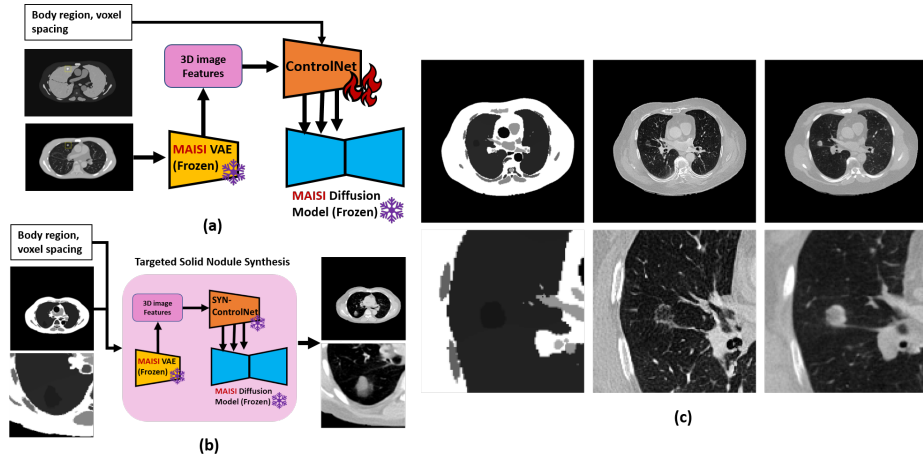


Fig. 6. Targeted nodule synthesis using simulated data. (a) MAISI-ControlNet fine-tuned with simulated data. (b) SYN-ControlNet generates targeted solid nodule CTs. (c) The first column shows the input body mask with a nodule for ControlNet, while the second and third columns display synthetic CT outputs from MAISI-ControlNet and SYN-ControlNet, respectively. The first row presents axial slices, and the second row zooms into the generated nodules. SYN-ControlNet enables nodule synthesis with specific nodule type.

4 Advantages, Limitations and Future Directions

SYN-LUNGS provides a structured approach to AI model training by integrating anatomy-informed simulated data with real-world clinical imaging characteristics. Our results demonstrate that **clinical + simulated** training consistently improves performance across multiple tasks. Nodule detection generalizes better to external dataset (DLCSD24), and segmentation models fine-tuned with SYN-LUNGS achieve higher Dice scores, especially for small nodules [1,3]. In malignancy classification, statistically labeled simulated nodules boosted performance through controlled augmentation. SYN-LUNGS also fine-tunes generative models, as shown by SYN-ControlNet [3], enabling anatomically consistent nodule generation. The digital human twins and dataset can be requested at

<https://cvit.duke.edu/resources/>, and model weights, training, and evaluation scripts will be available at <https://github.com/fitushar/SYN-LUNGS>. This study has limitations. The dataset includes 1000+ CT scans and 3000+ nodules, but unique digital twins remain limited due to full-chest modeling complexity. A new pipeline is in development to streamline this process. Statistical malignancy labeling, based on NLST[4], lacks biological modeling, and nodules are currently restricted to solid types, requiring expansion to semi-solid and ground-glass. The simulation pipeline mimics two NLST-era vendor configurations, and can be expanded with newer, vendor-specific imaging systems including photon-counting CT. Expanding SYN-ControlNet [3] to generate diverse lung abnormalities and increasing scanner diversity will further enhance its clinical relevance.

5 Conclusion

The SYN-LUNGS framework demonstrates improvements in detection, segmentation, and classification, establishing a foundation for future research aimed at enhancing rare disease representation and model reliability in clinical lung nodule assessment.

6 Acknowledgment

This work was funded in part by the National Institutes of Health (P41-EB028744, R01EB001838, R01HL155293). We also thank MONAI and NVIDIA for providing open-access code resources that supported this research.

References

1. He, Y., et al.: VISTA3D: A Unified Segmentation Foundation Model For 3D Medical Imaging. arXiv preprint [arXiv:2406.05285](https://arxiv.org/abs/2406.05285) (2024), <https://arxiv.org/abs/2406.05285>
2. Kiraly, A.P., et al.: Assistive AI in Lung Cancer Screening: A Retrospective Multi-national Study in the United States and Japan. *Radiology: Artificial Intelligence* **6**(3), e230079 (2024). <https://doi.org/10.1148/ryai.230079>
3. Guo, P., Zhao, C., Yang, D., Xu, Z., Nath, V., et al.: MAISI: Medical AI for Synthetic Imaging. arXiv preprint [arXiv:2409.11169](https://arxiv.org/abs/2409.11169) (2024), <https://arxiv.org/abs/2409.11169>
4. National Lung Screening Trial Research Team, Aberle, D.R., et al.: Reduced lung-cancer mortality with low-dose computed tomographic screening. *The New England Journal of Medicine* **365**(5), 395–409 (2011). <https://doi.org/10.1056/NEJMoa1102873>
5. Setio, A.A.A., et al.: Validation, comparison, and combination of algorithms for automatic detection of pulmonary nodules in computed tomography images: The LUNA16 challenge. *Medical Image Analysis* **42**, 1–13 (2017). <https://doi.org/10.1016/j.media.2017.06.015>

6. Wang, A., Tushar, F.I., Harowicz, M.R., Lafata, K.J., Taylor, T.D., Lo, J.Y.: Duke Lung Cancer Screening Dataset 2024 (1.1) [Data set]. Zenodo (2024). <https://doi.org/10.5281/zenodo.13799069>
7. Tushar, F.I., et al.: AI in Lung Health: Benchmarking Detection and Diagnostic Models Across Multiple CT Scan Datasets. arXiv preprint **arXiv:2405.04605** (2024), <https://arxiv.org/abs/2405.04605>
8. Antonelli, M., Reinke, A., Bakas, S., et al.: The Medical Segmentation Decathlon. *Nature Communications* **13**(1), 4128 (2022). <https://doi.org/10.1038/s41467-022-31801-3>
9. Chen, Q., Chen, X., Song, H., Xiong, Z., Yuille, A., Wei, C., Zhou, Z.: Towards Generalizable Tumor Synthesis. In: *Proceedings of the IEEE/CVF Conference on Computer Vision and Pattern Recognition*, pp. 11147–11158 (2024)
10. Dahal, L., et al.: XCAT-3.0: A Comprehensive Library of Personalized Digital Twins Derived from CT Scans. arXiv preprint **arXiv:2405.11133** (2024), <https://arxiv.org/abs/2405.11133>
11. Sauer, T.J., Samei, E.: Modeling dynamic, nutrient-access-based lesion progression using stochastic processes. In: Schmidt, T.G., Chen, G.-H., Bosmans, H. (eds.) *Medical Imaging 2019: Physics of Medical Imaging*, vol. 10948, 1094850. SPIE, International Society for Optics and Photonics (2019). <https://doi.org/10.1117/12.2513201>
12. McCabe, C., Solomon, J., Segars, W.P., Abadi, E., Samei, E.: Synthesizing heterogeneous lung lesions for virtual imaging trials. In: Fahrig, R., Sabol, J.M., Li, K. (eds.) *Medical Imaging 2024: Physics of Medical Imaging*, vol. 12925, 129251N. SPIE, International Society for Optics and Photonics (2024). <https://doi.org/10.1117/12.3006199>
13. Abadi, E., Harrawood, B., Sharma, S., Kapadia, A., Segars, W.P., Samei, E.: DukeSim: A Realistic, Rapid, and Scanner-Specific Simulation Framework in Computed Tomography. *IEEE Transactions on Medical Imaging* **38**(6), 1457–1465 (2019). <https://doi.org/10.1109/TMI.2018.2886530>
14. Badano, A., et al.: Evaluation of digital breast tomosynthesis as replacement of full-field digital mammography using an in silico imaging trial. *JAMA Network Open* **1**(7), e185474 (2018). <https://doi.org/10.1001/jamanetworkopen.2018.5474>
15. Abadi, E., et al.: Virtual clinical trials in medical imaging: a review. *Journal of Medical Imaging* **7**(4), 042805 (2020). <https://doi.org/10.1117/1.JMI.7.4.042805>
16. Tushar, F.I., et al.: Virtual lung screening trial (VLST): An in silico study inspired by the national lung screening trial for lung cancer detection. *Medical Image Analysis* **103576** (2025), <https://doi.org/10.1016/j.media.2025.103576>
17. Tushar, F.I., et al.: Virtual vs. reality: external validation of COVID-19 classifiers using XCAT phantoms for chest computed tomography. In: Drukker, K., Iftekharuddin, K.M. (eds.) *Medical Imaging 2022: Computer-Aided Diagnosis*, vol. 12033, 1203305. SPIE, International Society for Optics and Photonics (2022). <https://doi.org/10.1117/12.2613010>
18. Abadi, E., Segars, W.P., Sturgeon, G.M., Roos, J.E., Ravin, C.E., Samei, E.: Modeling lung architecture in the XCAT series of phantoms: physiologically based airways, arteries and veins. *IEEE Transactions on Medical Imaging* **37**(3), 693–702 (2018). <https://doi.org/10.1109/TMI.2017.2769640>
19. Abadi, E., et al.: Airways, vasculature, and interstitial tissue: anatomically informed computational modeling of human lungs for virtual clinical trials. In: Flohr, T.G., Lo, J.Y., Schmidt, T.G. (eds.) *Medical Imaging 2017: Physics of Medical Imaging*, vol. 10132, 101321Q. SPIE, International Society for Optics and Photonics (2017). <https://doi.org/10.1117/12.2254739>

20. Sauer, T.J., McCabe, C., Abadi, E., Samei, E., Segars, W.P.: Surface-based anthropomorphic bone structures for use in high-resolution simulated medical imaging. *Physics in Medicine & Biology* **69**(1), 015023 (2023). <https://doi.org/10.1088/1361-6560/acfc69>
21. MONAI Project: MONAI Detection Tutorial. <https://github.com/Project-MONAI/tutorials/tree/main/detection>, last accessed 2024/02/25.
22. Pai, S., et al.: Foundation model for cancer imaging biomarkers. *Nature Machine Intelligence* **6**(3), 354–367 (2024). <https://doi.org/10.1038/s42256-024-00707-y>
23. Chen, S., Ma, K., Zheng, Y.: Med3D: Transfer Learning for 3D Medical Image Analysis. arXiv preprint **arXiv:1904.00625** (2019), <https://arxiv.org/abs/1904.00625>
24. Isensee, F., et al.: nnU-Net: a self-configuring method for deep learning-based biomedical image segmentation. *Nature Methods* **18**(2), 203–211 (2021). <https://doi.org/10.1038/s41592-020-01008-z>
25. Tushar, F.I., Vancoillie, L., Ghosh, D., Lafata, J.K., Lo, J.: Beyond Detection: Bridging the Gap between Virtual Imaging Trials and Clinical Impact. In: *Proc. Virtual Imaging Trials in Medicine 2024*, 2024/05/08 (2024).